Supplementary Material to: *Brief Communication: Detection of glacier surge activity using cloud computing of Sentinel-1 radar data*

Paul Leclercq, Andreas Kääb, Bas Altena

1 Global results

Here we present in more detail the global results of our detection of glaciers with surge activity. Fig. S1 shows the global coverage of the Sentinel-1 NDI images for the period 2018–2019 as calculated from the available data in Google Earth Engine (GEE). To be able to calculate such a difference image we need radar backscatter amplitude imagery in both winters (defined as January – March for the Northern Hemisphere and June – August for the Southern Hemisphere), 2018 as well as in winter 2019. The VH polarized imagery in GEE covers a large fraction of the global land area. But northeast Canada, Greenland, the eastern edge of Svalbard, Franz Josef Land, Novaya Zemlya, and eastern parts of Severnya Zemlya are not covered by this in either ascending or descending path. In order to cover these glacierized area, we need to select the HV polarized images that gives us almost complete coverage of the Canadian Arctic and most of Greenland's local glaciers in descending path. There are no images over Antarctica. In ascending orbit we can complement with parts of Greenland and Svalbard. Both with VH and HV polarization, the descending orbit gives most coverage. So we use descending orbit as default and use ascending orbit images to complement for the areas not covered by descending orbit, and a few cases where the mountain topography makes ascending more suitable than descending orbit (see also Section 2). Combination of ascending and descending paths leaves some glacierized areas, such as Franz Josef Land and smaller areas in Greenland and Canadian Arctic, not covered for the 2018-2019 data. Where possible, we use NDI images from other years to fill data gaps.

In total we find surge activity for 69 glaciers and glacier tributaries in the study period 2018–2019. Table S1 provides a list of the surge-type glaciers we find, including the surge classification given in the RGI [RGI Consortium, 2017] based on Sevestre and Benn [2015]. Fig. S2 shows the distribution of these glaciers on a world map. The majority of the surges we have detected are found in Alaska (18 glaciers with surge activity), Svalbard (14) and High-Mountain Asia (13). In both the table and the figure, the glaciers are grouped based on whether the surge activity detection is based on increased backscatter (31 cases), decreased backscatter (29), or a combination of increased and decreased radar backscatter (9). In the table we have also included the 18 glaciers that show a change in backscatter but for which we found it unclear if this was caused by surge activity.

Of the 69 glaciers on which we have detected surge activity, 3 are classified as possible surge type, 5 are classified as probable surge type, 16 are classified as observed surging, 10 are classified as no evidence of surge, and 35 have no surge-type classification in the RGI. This means that almost two-thirds of the glaciers for which we detect surge activity in our study period 2018-2019 have not been identified as surge-type glaciers previously. There are large regional differences in the classification of the surge-type glaciers we detect. Out of the 14 surging glaciers we found in Svalbard, 12 are classified in RGI as having either direct or indirect evidence of surge activity, but

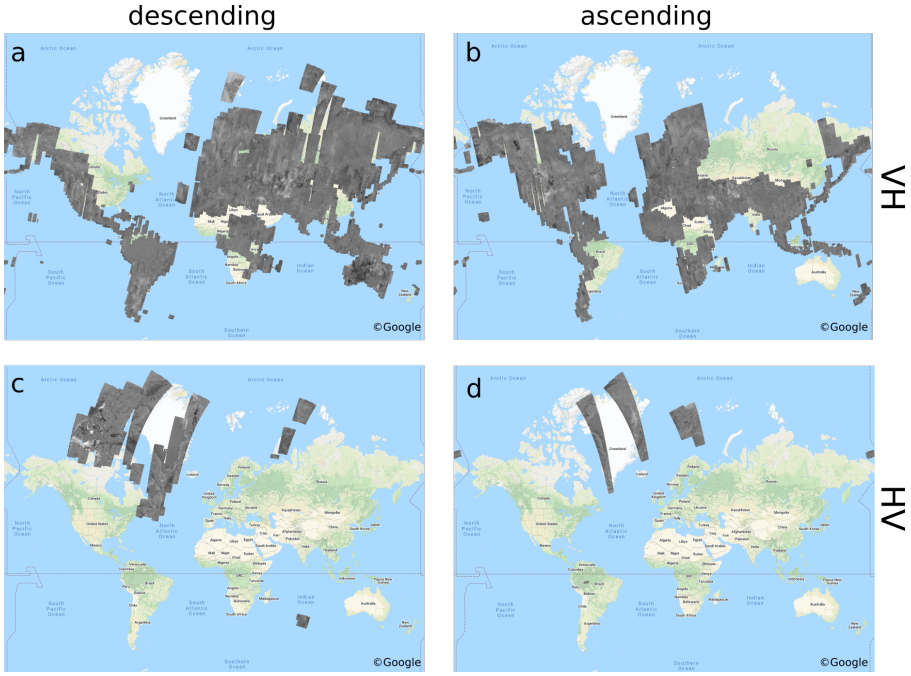

Figure S1: Coverage (in grey) of NDI images based on Sentinel-1 radar images as available in © Google Earth Engine for the periods used in this study, 1st January 2018 – 1st April 2018 and 1st January 2019 – 1st April 2019: **a**) VH polarization, descending orbit **b**) VH polarization, ascending orbit **c**) HV polarization, descending orbit **d**) HV polarization, ascending orbit.

16 of the 18 glaciers we find surging in Alaska do not have a surge classification in the RGI. 6 out of the 10 glaciers that we find to have surge activity while the RGI classification states no evidence of such activity are located in RGI region South Asia (West).

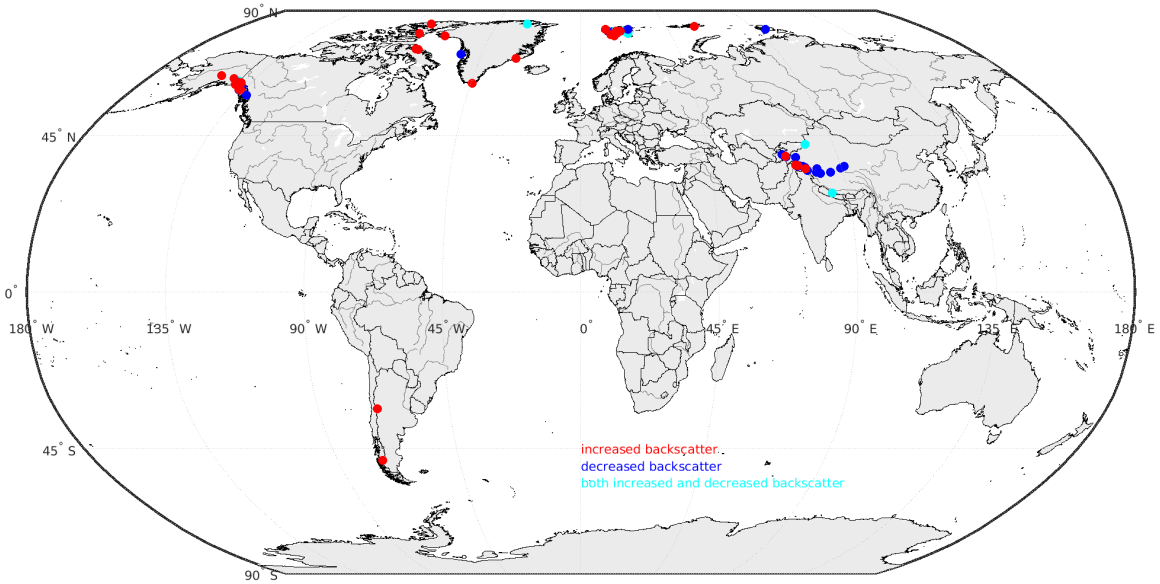

Figure S2: Global overview of the location of glaciers with surge activity found in this study. Glaciers for which the surge activity is derived from a backscatter increase between winter 2018 and winter 2019 are shown in **red**, a decrease in backscatter in **blue**, and glaciers which show both types of changes, an increase as well as parts with a decrease in backscatter, are shown in **cyan**.

Table S1: GLIMS ID, RGI ID, name, region, latitude, longitude, and surge type as given in the RGI, for the glaciers where we have detected surge activity over the year 2018-2019 from Sentinel-1 radar images. Sometimes a local inventory code is given as a name, if both inventory code and a name are given in the GLIMS data set [GLIMS and NSIDC, 2015 (updated 2018)], we have only displayed the name. If no name is given, we have put a "-". Latitude and Longitude are the coordinates of the glacier centre point as given in GLIMS. Surge type classifies the surge activity from Sevestre and Benn [2015] as given in the RGI: 0 no evidence of surge; 1 surge possible; 2 surge probable; 3 observed surge; 9 not assigned.

GLIMS ID	RGI ID	name	region	latitude	longitude	surge type
increased surface backscatter						
G209330E63184N	RGI60-01.22169	Muldrow Glacier	Alaska	63.184	-150.670	3
G216046E62056N	RGI60-01.15772	-	Alaska	62.056	-143.954	9
G220578E60873N	RGI60-01.16198	Kluane Glacier ++	Alaska	60.873	-139.422	9
G219251E60184N	RGI60-01.23649	Agassiz Glacier	Alaska	60.184	-140.749	9
G220560E60074N	RGI60-01.26736	Valerie Glacier	Alaska	60.074	-139.440	9
G222370E58832N	RGI60-01.20984	Fairweather Glacier	Alaska	58.832	-137.630	9
G223186E58746N	RGI60-01.20783	Reid Glacier	Alaska	58.746	-136.814	9
G223237E58554N	RGI60-01.20796	Brady Glacier	Alaska	58.554	-136.763	9
G278750E77768N	RGI60-03.01713	-	Canadian Arctic North	77.768	-81.250	0
G279683E81662N	RGI60-03.03389	Yelverton	Canadian Arctic North	81.662	-80.317	0
G284690E71788N	RGI60-04.04021	-	Canadian Arctic South	71.788	-75.310	9
G283518E71938N	RGI60-04.05006	-	Canadian Arctic South	71.938	-76.482	9
G330976E68786N	RGI60-05.13667	-	Greenland	68.786	-29.024	9
G315572E60586N	RGI60-05.04143	-	Greenland	60.586	-44.428	9
G292408E76864N	RGI60-05.08054	-	Greenland	76.864	-67.592	9
G012697E79319N	RGI60-07.01494	Monacobreen	Svalbard	79.319	12.697	3
G020098E78757N	RGI60-07.00892	Sonklarbreen +	Svalbard	78.757	20.098	3
G018042E78675N	RGI60-07.01506	Negribreen +	Svalbard	78.675	18.042	3
G018098E77802N	RGI60-07.00276	Arnesenbreen	Svalbard	77.802	18.098	1
G017697E77678N	RGI60-07.00296	Strongbreen	Svalbard	77.678	17.697	2
G016757E76881N	RGI60-07.00299	Pulkovbreen	Svalbard	76.881	16.757	3
G015037E77377N	RGI60-07.00228	Recherchebreen	Svalbard	77.377	15.037	3
G016777E76955N	RGI60-07.00440	Svalisbreen	Svalbard	76.955	16.777	0
G059756E80623N	RGI60-09.00747	Tyndall Ice Cap†	Franz Josef Land	80.623	59.756	9
G071776E38900N	RGI60-13.19763	Gando	Central Asia	38.900	71.776	3
G074679E36413N	RGI60-14.05446	Shispher * ++	South Asia (West)	36.413	74.679	3
G074496E36424N	RGI60-14.03017	Muchuhar **	South Asia (West)	36.424	74.496	0
G075270E36240N	RGI60-14.03334	Yazgil Glacier	South Asia (West)	36.240	75.270	0
G077527E35330N	RGI60-14.05890	Rimo Glacier	South Asia (West)	35.330	77.527	3

Table S1: (continued)

GLIMS ID	RGI ID	name	region	latitude	longitude	surge type
G286499E48466S	RGI60-17.06074	Jorge Montt	Southern Andes	-48.466	-73.501	9
G290243E33492S	RGI60-17.13796	Tupungato Sur ***	Southern Andes	-33.492	-69.757	3
decreased surface backscatter						
G219611E60880N	RGI60-01.26738	Walsh Glacier	Alaska	60.880	-140.389	9
G219611E60880N	RGI60-01.26738	Walsh Glacier ****	Alaska	60.880	-140.389	9
G220204E60098N	RGI60-01.14391	Turner Glacier	Alaska	60.098	-139.796	9
G220740E60158N	RGI60-01.14443	Hubbard Glacier	Alaska	60.158	-139.260	9
G221417E60065N	RGI60-01.16122	Fisher Glacier	Alaska	60.065	-138.583	9
G223292E59259N	RGI60-01.26729	Tkope Glacier	Alaska	59.259	-136.708	9
G222793E58546N	RGI60-01.20791	La Perouse Glacier	Alaska	58.546	-137.207	1
G227688E56917N	RGI60-01.03622	LeConte Glacier	Alaska	56.917	-132.312	9
G305818E70120N	RGI60-05.01879	GL2U1HE11013	Greenland	70.120	-54.182	2
G013901E78579N	RGI60-07.00465	Wahlenbergbreen	Svalbard	78.579	13.901	2
G015616E77394N	RGI60-07.00241	Penckbreen	Svalbard	77.394	15.616	1
G024396E79406N	RGI60-07.00026	Bråsvellbreen	Svalbard	79.406	24.396	0
G095377E79354N	RGI60-09.00971	Vavilov Ice Cap	Novaya Zemlya	79.354	95.377	9
G070672E39517N	RGI60-13.17829	Zeravshan Glacier	Central Asia	39.517	70.672	9
G071322E38959N	RGI60-13.19863	SU5X14309085	Central Asia	38.959	71.322	2
G071954E38799N	RGI60-13.19758	Shocalscogo *****	Central Asia	38.799	71.954	2
G071925E38770N	RGI60-13.19075	Vanchdara	Central Asia	38.770	71.925	3
G075248E38558N	RGI60-13.41792	CN5Y663D0004	Central Asia	38.558	75.248	9
G080875E34263N	RGI60-13.51630	CN5Z413E0008	Central Asia	34.263	80.875	9
G082268E34005N	RGI60-13.51476	CN5Z412C0007	Central Asia	34.005	82.268	9
G085885E34389N	RGI60-13.53958	CN5Z514H0005	Central Asia	34.389	85.885	9
G089776E35593N	RGI60-13.49228	CN5Z211I0007	Central Asia	35.593	89.776	9
G091032E36060N	RGI60-13.33983	Monuomaha Glacier	Central Asia	36.060	91.032	9
G081483E35351N	RGI60-13.37603	CN5Y641F0046	Central Asia	35.351	81.483	9
G075492E36141N	RGI60-14.04404	Khurdopin Glacier	South Asia (West)	36.141	75.492	3
G074991E35994N	RGI60-14.04638	Chogo Glacier	South Asia (West)	35.994	74.991	0
G076794E36050N	RGI60-14.06390	-	South Asia (West)	36.050	76.794	0
G077483E35705N	RGI60-14.07022	- ++	South Asia (West)	35.705	77.483	0
G077896E34827N	RGI60-14.08555	North Kunchhang Glacier I	South Asia (West)	34.827	77.898	3
combination of decreased and increased surface backscatter						
G218909E61392N	RGI60-01.17183	Klutlan Glacier	Alaska	61.392	-141.091	9
G222709E58921N	RGI60-01.20891	Margerie Glacier	Alaska	58.921	-137.291	9
G331218E81833N	RGI60-05.10033	-	Greenland	81.833	-28.782	9
G017497E78572N	RGI60-07.01458	Tunabreen	Svalbard	78.572	17.497	3
G020757E78746N	RGI60-07.00897	Ganskijbreen	Svalbard	78.746	20.757	3
G023608E77828N	RGI60-07.01554	Stonebreen	Svalbard	77.828	23.608	3
G079956E42288N	RGI60-13.04933	-	Central Asia	42.288	79.956	9
G076773E36052N	RGI60-14.06360	-	South Asia (West)	36.052	76.773	0
G084759E28427N	RGI60-15.04151	-	South Asia (East)	28.427	84.759	9
change in surface backscatter, possibly surge but not classified as such						
G274606E76824N	RGI60-03.01897	Sydkap	Canadian Arctic North	76.824	-85.394	3
G280449E77998N	GI60-03.01710	Wykeham Glacier South	Canadian Arctic North	77.998	-79.551	3
G284855E71673N	RGI60-04.03879	-	Canadian Arctic South	71.673	-75.145	9
G283422E71906N	RGI60-04.05008	-	Canadian Arctic South	71.906	-76.578	9
G283848E72097N	RGI60-04.05004	-	Canadian Arctic South	72.097	-76.152	9
G322065E82674N	RGI60-05.10749	-	Greenland	82.674	-37.935	9
G328550E68813N	-	Frederiksborg Glacier	Greenland	68.813	-31.450	9
G330613E68651N	RGI60-05.13667	Rosenborg Glacier	Greenland	68.651	-29.387	9
G331192E68888N	RGI60-05.13667	Kronborg Glacier	Greenland	68.888	-28.808	9
G307955E65949N	RGI60-05.00310	-	Greenland	65.949	-52.045	9
G291220E76967N	RGI60-05.08041	-	Greenland	76.967	-68.780	9
G066985E76524N	RGI60-09.00072	Severny Island Ice Cap	Novaya Zemlya	76.524	66.985	9
G082378E35679N	RGI60-13.36881	CN5Y636I0024	Central Asia	35.679	82.378	9
G082168E35513N	RGI60-13.37003	CN5Y636J0029	Central Asia	35.513	82.168	9
G074654E36547N	RGI60-14.02150	Batura Glacier	South Asia (West)	36.547	74.654	0
G074328E34947N	RGI60-14.20187	-	South Asia (West)	34.947	74.328	9
G084341E28748N	RGI60-15.04715	-	South Asia (East)	28.748	84.341	9
G084341E28748N	RGI60-15.04715	-	South Asia (East)	28.561	84.014	9

comments	
†	based on NDI image from years 2017–2018
*	called "Hassanabad Glacier I" in GLIMS and RGI
**	called "Hassanabad Glacier II" in GLIMS and RGI
***	name in RGI is given as "Tupungato Sur/Tunuyan"
****	a tributary to Walsh glacier
*****	RGI name is SU5X14309227 Garmo
+	used as example in results section and shown in Fig. 2
++	used as example Section 2 and shown in Fig. S3

2 Descending and ascending path

The Sentinel-1 constellation is in a sun-synchronous orbit with and inclination of 98.18° and data are available from both ascending and descending path. As mentioned in the previous Section, we use mainly radar images from descending paths in the global study. The main reason to use the descending path is the better coverage of these images in GEE. In general we find no difference in the results between using images from ascending and descending paths where both are available, although in some particular occasions the two can provide complementing information. In Fig. S3 we show a comparison between the normalized difference index (NDI) images from descending and those from ascending paths. The first example in Fig. S3 (a–c) is the NDI image for the same area in the Pamirs as used in Fig. 1. As the line of sight is different, the valley walls that give a noisy signal and the ones that are in the radar shadow are different for the ascending and descending NDI images. But the NDI for the glacierized areas are very similar, such that the detection of surge activity is the same for the NDI derived from ascending path as it is for the NDI image from descending path.

The second example (Fig. S3 d–f) shows the NDI for both descending and ascending path over Shispher glacier and the Sentinel-2 image for the same area in the Karakoram, Pakistan. Shispher Glacier is known to have surged recently [Rashid et al., 2020]. The surging glacier tongue blocked the river from a tributary valley which led to an ice-dammed lake that threatened the downstream village of Hassanabad and the Karakoram Highway. Shispher glacier is surrounded by extremely steep terrain. The NDI images shown in Fig. S3 show a lot of noise around the highest peaks. On the descending NDI image shown in Fig. S3, the whole mountain flank to the west of the glacier tongue is very bright as well, while this part is not covered by ice. This mountain flank is under SAR foreshortening and layover that appears stretched out through the orthorectification process. Some artificial differences in this process create strong differences in the backscatter stack maxima. This example highlights that differences in radar backscatter brightness can be caused by acquisition and processing effects in addition to natural ones. In this specific case, the ascending geometry creates much less such problems and the surge can be detected much more clearly. The Shispher Glacier example also demonstrates how glacier lake changes can be detected using our method. Changes in the ice-dammed lake to the west of the glacier tongue are clearly visible as backscatter changes in the descending path (for the ascending path the lake lies in the radar shadow), based on the fact that smooth water surfaces create particularly strong forward-scattering, and thus reduced backscatter.

Fig. S3 g–i shows the results of a nameless glacier with GLIMS ID G077483E35705N in the Karakoram Range, China. This glacier provides an example of surge activity detected from a decrease in backscatter. The last of the examples (Fig. S3 j–l) shows the NDI of Kluane Glacier, Alaska, which has a clear increase in radar backscatter.

The noise pattern in the difference images from the ascending paths is clearly different from that of the descending paths. As the radar signal comes from the opposite direction, the effects of overlay, foreshortening and shading differ. This is most prominent in the example of Shispher Glacier, due to the extreme topography of the Karakorum where it is located. In the particular case of Shispher Glacier, the signal from the glacier surge is much better discernible from the acquisition and processing effects in the image taken in ascending path. However, for the vast majority of the detected surges, as in the three other examples shown here, the signal from the glacier surface is almost identical for both paths and the surge detection is not influenced by the choice of path azimuth. This also indicates that the surge detection is not dependent on the angle between direction of glacier flow and radar satellite azimuth, likely due to an over large parts chaotic nature of surge-related crevasses, without directional preference.

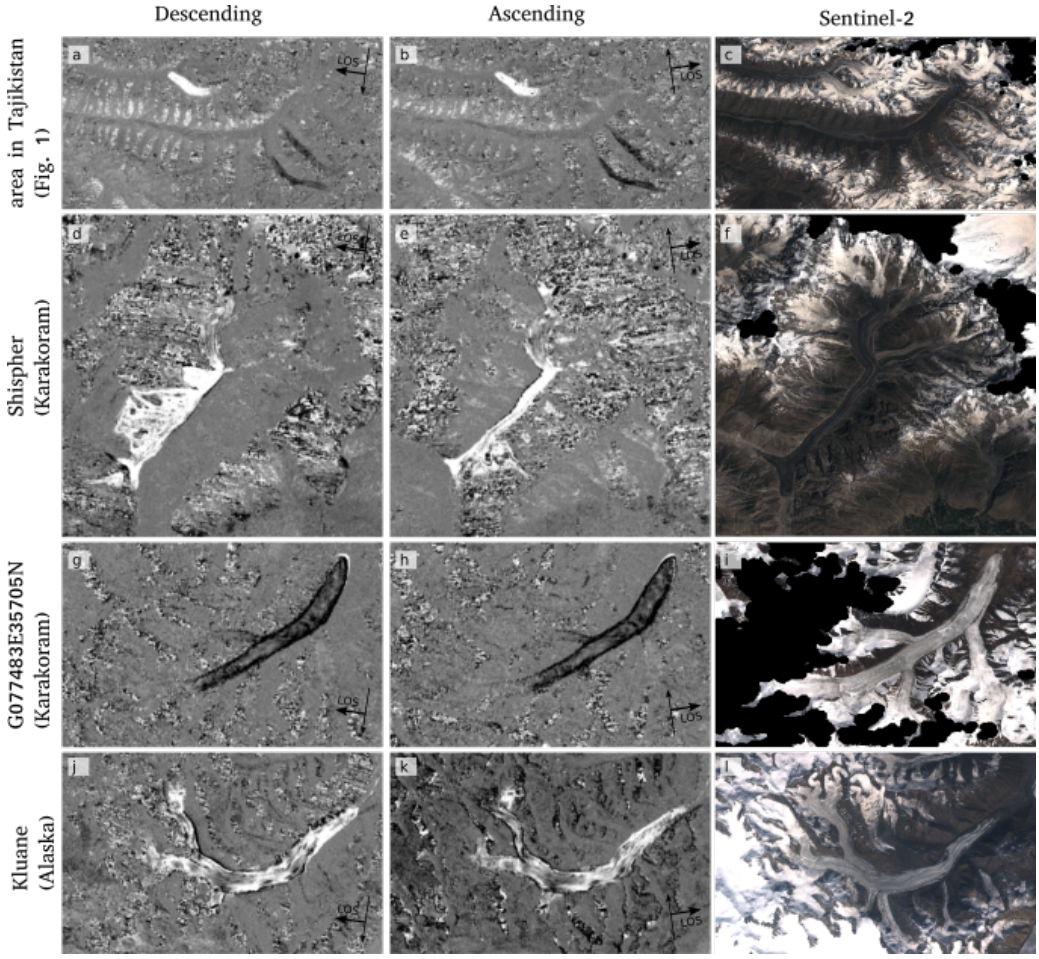

Figure S3: Examples of 2018 – 2019 NDI images from descending path (**a**,**d**,**g**,**j**), as used for the global results in this paper, and ascending path (**b**,**e**,**h**,**k**) of Sentinel-1, and the optical Sentinel-2 summer 2019 image (**c**,**f**,**i**,**l**) of the same area. The Sentinel-2 images have a cloud mask in black. In the NDI images the Line Of Sight (LOS) for descending and ascending path is shown. The location of the upper example (**a** – **c**) is identical to Fig. 1. The second to fourth example shows the NDI images of Shispher Glacier, the glacier with GLIMS ID G077483E35705N, both in the Karakoram Range, and Kluane Glacier, Alaska, respectively.

3 Other observed processes

As mentioned in the Discussion section, surge activity is not the only natural process that can cause temporal difference in radar backscatter brightness on glaciers. Although glacier surges are the main focus of the paper, we would like to stress that the method we propose here to detect glacier surges also has potential in other fields of geoscience. Further exploration of the method in terms of different stack statistics and other differencing periods than the yearly interval we have used could further improve the detection of a range of other processes. We have observed difference in backscatter brightness in accumulation areas where we suspect changing firn conditions to be the cause, changes in glacial lakes, change in sea-ice conditions, landslides, a glacier detachment, and snow avalanche activity. Figure S4 shows four examples of these processes.

The first image of the figure (Fig. S4a) shows the 2018-2019 normalized difference image where we observe increased backscatter from the surface of a nameless glacier in the Alaska Range, Alaska (GLIMS ID G213541E63316N) that is similar to the signal of a glacier surge. Studying the Sentinel-2 optical images of summer 2017 (Fig. S4b) and summer 2019 (Fig. S4c) it becomes clear that

this increase in radar backscatter is caused by the deposits of a large landslide, rather than by surge activity. The landslide is first seen on the Sentinel-2 image from the 7th of July 2018, and must have happened between the Sentinel-2 acquisitions on the 6th and the 7th of July 2018. The landslide deposits have a higher roughness and thus backscatter than the underlying glacier surface, which leads to an increase in the backscatter brightness from winter 2018, before the event, to winter 2019.

The second example (Fig. S4 d-f) shows both a landslide and snow avalanches on Tlikakila Glacier Fork, Alaska Range. Again, the landslide causes an increase in radar backscatter brightness, and must have occurred between acquisition of the last radar images of winter 2018 and the acquisition of the summer 2018 Sentinel-2 composite image shown in Fig. S4f. Note that there is a band of no increase in backscatter where the landslide covers the middle moraine on the glacier, i.e. did not change roughness and backscatter. In addition to the landslide, we observed several small patches of decreased radar backscatter. These correspond to snow patches that are visible in summer 2018 (Fig. S4f) but not in summer 2017 (Fig. S4e) or summer 2019 (not shown) and we believe to be the remainders of snow avalanche deposits. These patches of decreased radar backscatter can thus be explained by avalanche activity during the winter of 2018 that increased the stack maximum backscatter in this period on the avalanche deposits. During summer, the avalanche deposits melted and during the following winter there was less or no avalanche activity at these locations, such that the stack maximum backscatter in this period was lower than it was the winter before. In our global analysis we find a large number of snow avalanche signs, over glaciers and around.

The third example (Fig. S4 g-i) shows the observation of the glacier detachment of Sedongpu Glacier in eastern Tibet with GLIMS ID G094940E29811N that occurred in October 2018 [Kääb et al., 2021]. On the NDI image we see clear changes in radar backscatter on the lower part of the glacier and in the main valley where deposits of the glacier detachment blocked the Yarlung Tsangpo river. Comparison of two composite Sentinel-2 images, one from autumn (October – December, a season with less clouds than summer) 2017 and the second from autumn 2018, show that in autumn 2018 the lower part of the glacier has collapsed and that the river in the valley beneath has been filled with ice and rock debris.

A last example (Fig. S4 j-l) shows a decrease in radar backscatter between winter 2018 and winter 2019 over the firn area of Langjökull, Iceland. This decrease in radar backscatter is prominent on all Icelandic glaciers for this year, and changes in backscatter in glacier firn areas can be found in all regions. We believe these changes have to do with firn processes such as changes in the melt water content, formation of superimposed ice or ice lenses in the snow pack.

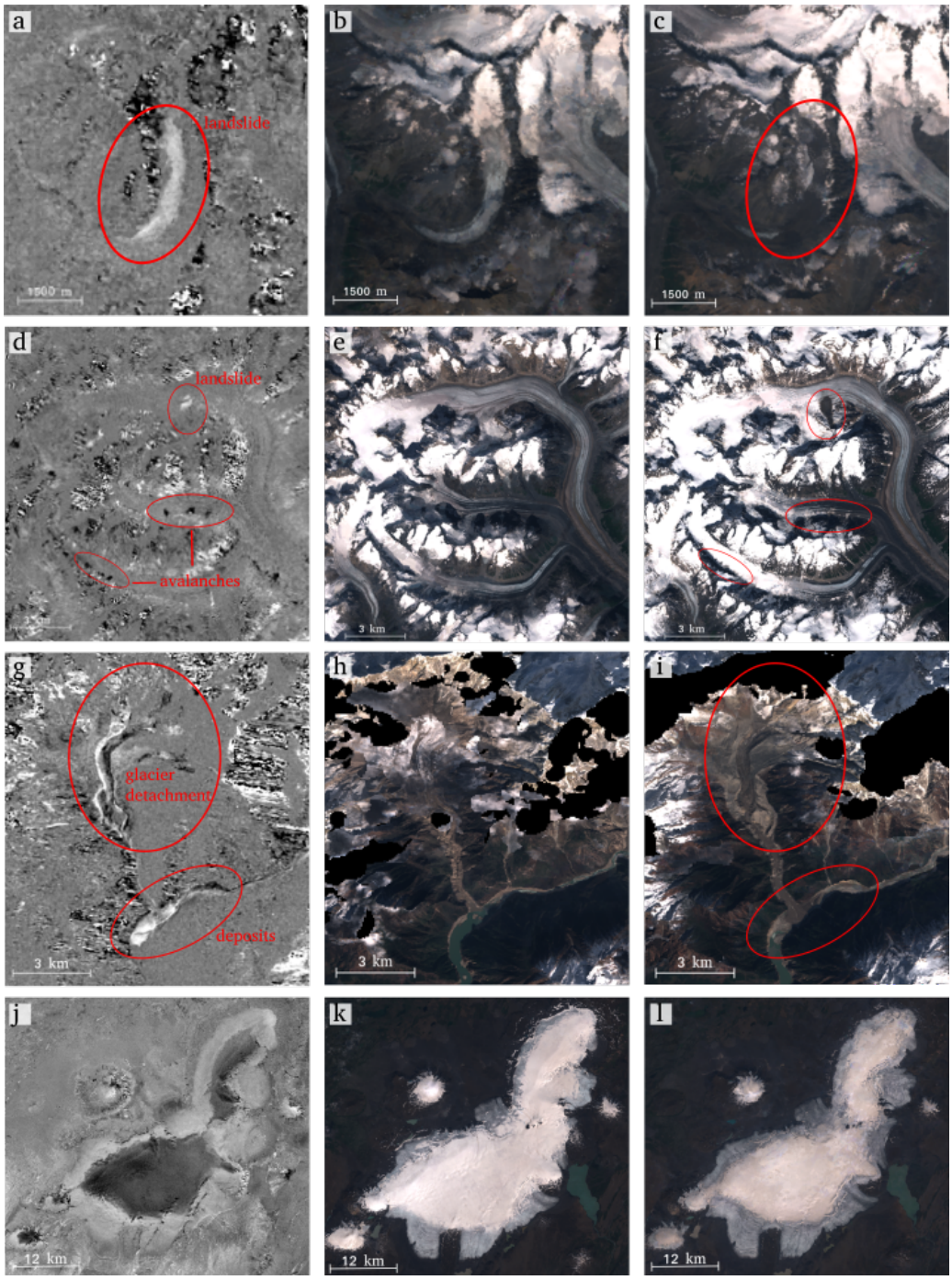

Figure S4: Examples of features other than surges visible in the NDI images. Here we show a landslide on a glacier with GLIMS ID G213541E63316N, Alaska Range (**a-c**); snow avalanches and another land slide on Tlikakila Glacier Fork, Alaska Range (**d-f**); the detachment of Sedongpu Glacier, Eastern Tibet (**g-i**); and decreased backscatter in the firn area of Langjökull, Iceland (**j-l**). Shown are the 2018-2019 NDI images (**a,d,g,j**), summer 2017 Sentinel-2 "before" images (**b,e,k**), autumn (october–december) 2017 Sentinel-2 "before" image (**h**), summer 2019 Sentinel-2 "after" image (**c,l**), summer 2018 Sentinel-2 "after" image (**f**), and autumn 2018 Sentinel-2 "after" image (**i**). The Sentinel-2 images have a cloud mask in black.

4 Comparison with surface velocity measurements

We compare the detection of surge activity from changing in Sentinel-1 radar backscatter with glacier surface velocity measurements of two regions, Svalbard and Alaska. The goal of this comparison is to determine whether the surges we detected can be confirmed by corresponding changes in observed glacier surface velocity. For Svalbard, we also check the velocity fields of all glaciers in the region for surges other than the ones we identified from radar backscatter differences that we may have missed with our method.

4.1 Svalbard velocity

Figure S5 shows own Sentinel-1 derived 12-day glacier velocity maps for Januaries 2018 and 2019, and December 2019 [see e.g. Strozzi et al., 2017, for details on the method], and the locations of surge activities from our backscatter-difference method. The increasing/decreasing surge activity of Monacobreen, Sonklarbreen, Negribreen, Arnesenbreen, Strongbreen, Recherchebreen, Svalisbreen, Wahlenbergbreen, Penckbreen and Tunabreen are cleary reflected in the velocity changes, mostly even at the scale depicted here. For Pulkovbreen and Ganskijbreen, the change in velocities is hard to measure and recognize due to the small size of the glaciers. The optical images, though, clearly show a surge of Ganskijbreen, and a weaker or partial surge for Pulkovbreen. The latter two glaciers are examples where the backscatter-based method makes surge detection easier compared to velocity change detection.

4.2 Alaska glacier surface velocity

In Alaska we use annual glacier surface velocity provided by NASA MeaSUREs ITS_LIVE project [Gardner et al., 2020]. ITS_LIVE generated surface velocity from optical satellite images using auto-RIFT [Gardner et al., 2018], and we use the annual velocity for the years 2015, 2016 and 2017 with a resolution of 120 m. We have to exclude the velocity field for 2018, as currently the data for this year have limited quality [Gardner pers. comm.]. This is due to a low number of scenes processed for this year so far. Still we expect that looking at the surface velocity in the years 2015 – 2017 will provide an indication of surges that we detect with radar images from the period winter 2018 – winter 2019. If a peak in surge activity is reached in the years 2015-2017, we should be able to detect a decrease in radar backscatter in 2018–2019. In addition, as shown in the example of Negribreen, Svalbard, increased radar backscatter can occur even after the peak in surface velocity.

Fig. S6 shows the annual velocity fields of the year 2015, 2016 and 2017 for the 8 glaciers where we observe an increase in radar backscatter in the period 2018 – 2019. For all glaciers except Reid Glacier the surface velocity shows a marked increase over the years 2015 – 2017. These velocity increases are consistent with our interpretation that the increased backscatter indicates a glacier surge. For Reid Glacier surface velocities are just slightly higher in 2017 than they are in the two proceeding years, such that there is no evidence for a glacier surge in the surface velocity data of this glacier.

For the glaciers we observe a decrease in the radar backscatter, the interpretation of the velocity fields, shown in Fig. S7, is less straightforward. For only three glaciers (Walsh Glacier,a tributary of Walsh Glacier, and Fisher Glacier), we find a strong decrease in surface velocity over the 2015 – 2017 period such that these glaciers can be interpreted as being at the end of a surge. Four glaciers (Turner Glacier, Hubbard Glacier, La Perouse Glacier, and Le Comte Glacier) exhibit an increase in glacier surface velocity in 2017. As we have no reliable data for the surface velocity in 2018, the year used for the radar backscatter analysis, we can not exclude that in this year the velocity

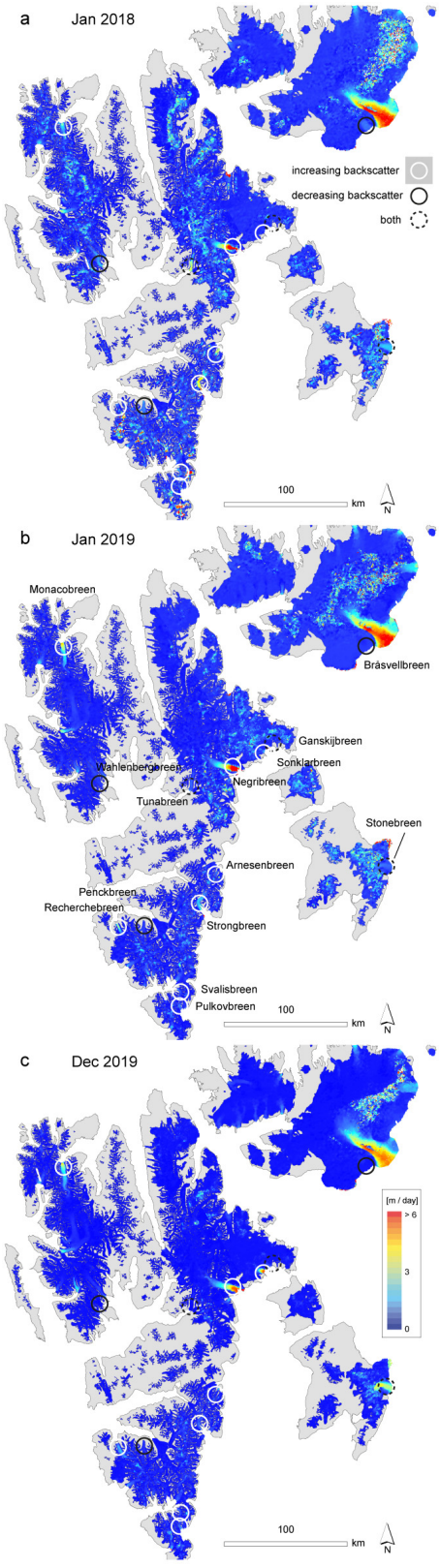

Figure S5: Sentinel-1 derived 12-day glacier velocity map for Svalbard for **a**) January 2018, **b**) January 2019, and **c**) December 2019. The locations of surge activities detected with our backscatter-difference method are shown with different circles: white for increasing backscatter, black for decreasing backscatter, and dotted circles for both increasing and decreasing backscatter over the study period winter 2018 – winter 2019.

and surface roughness dropped significantly again. That would be needed to explain a decrease in radar backscatter. In that case the surface roughness has to respond faster than we observed in our example of Negribreen. To conclude, Tkope Glacier has no marked change in glacier surface velocity.

For the 2 glaciers that showed both increased and decreased radar backscatter, the surface velocity is shown in Fig. S8. Margerie Glacier has much higher velocity in 2017 than it has in 2015 and 2016, which indicates a surge event like for the other glaciers we discuss above. For Klutlan Glacier, the ITS_LIVE data give a high velocity in 2015, after which the glacier flow is lower in 2016 and increases again in 2017. The velocity in 2017 is partly higher than in 2015 but more unevenly distributed over the glacier. We believe the lower surface velocity in 2016 could be due to a incorrect processing of the fast flow of this glacier, as Altena et al. [2019] find a continuous propagation of the surge bulge. The passage of the surge bulge can explain why we find both areas with increased radar backscatter as well as areas with decreased backscatter on the surface of Klutlan glacier.

ITS_LIVE velocity data also provide a formal uncertainty to the velocity fields. The uncertainty in the velocity for the glaciers we discuss here is shown in Figures S9–S11. Uncertainty in surface velocity is higher in the first two years (2015, 2016) than it is in 2017, and in general the uncertainty is much lower than the observed velocity for the glaciers of our interest, especially for the velocities in 2017, such that it is unlikely that the marked increases and decreases in surface velocity are due to measurement errors.

Based on the glacier surface velocity shown in Fig. S6 -S8, we can conclude that for 16 of the 18 glaciers the ITS_LIVE velocities support the detection of glacier surge activity from the normalized difference image of Sentinel-1 radar data, as the surface velocity has a significant change in the years 2015 to 2017. Two glaciers do not have a significant change in surface velocity during the years 2015 to 2017 that can support our surge activity observations from Sentinel-1. For both Reid Glacier and Tkope Glacier, the radar signal observed in 2018–2019 has disappeared in the 2019–2020 normalized difference image and the glacier extent seems nearly unchanged over the period 2017 – 2019. Therefore, we have most likely misinterpreted an increase and a reduction in backscatter, respectively, for surge activity while in fact it was caused by another process, most likely a process in the firn pack. To conclude, we should mention that if we look at Fig S6, we see in the surface velocity plots for the glacier with GLIMS ID G216046E62056N there are two glaciers that show a similar significant increase in surface velocity: glacier G216046E62056N in the centre of the plots and Copper Glacier (GLIMS ID G216225E62044N) to the east of it. However, we do not see a signal in the 2018–2019 normalised difference image for Copper Glacier, while we do see an increase in radar backscatter for glacier G216046E62056N.

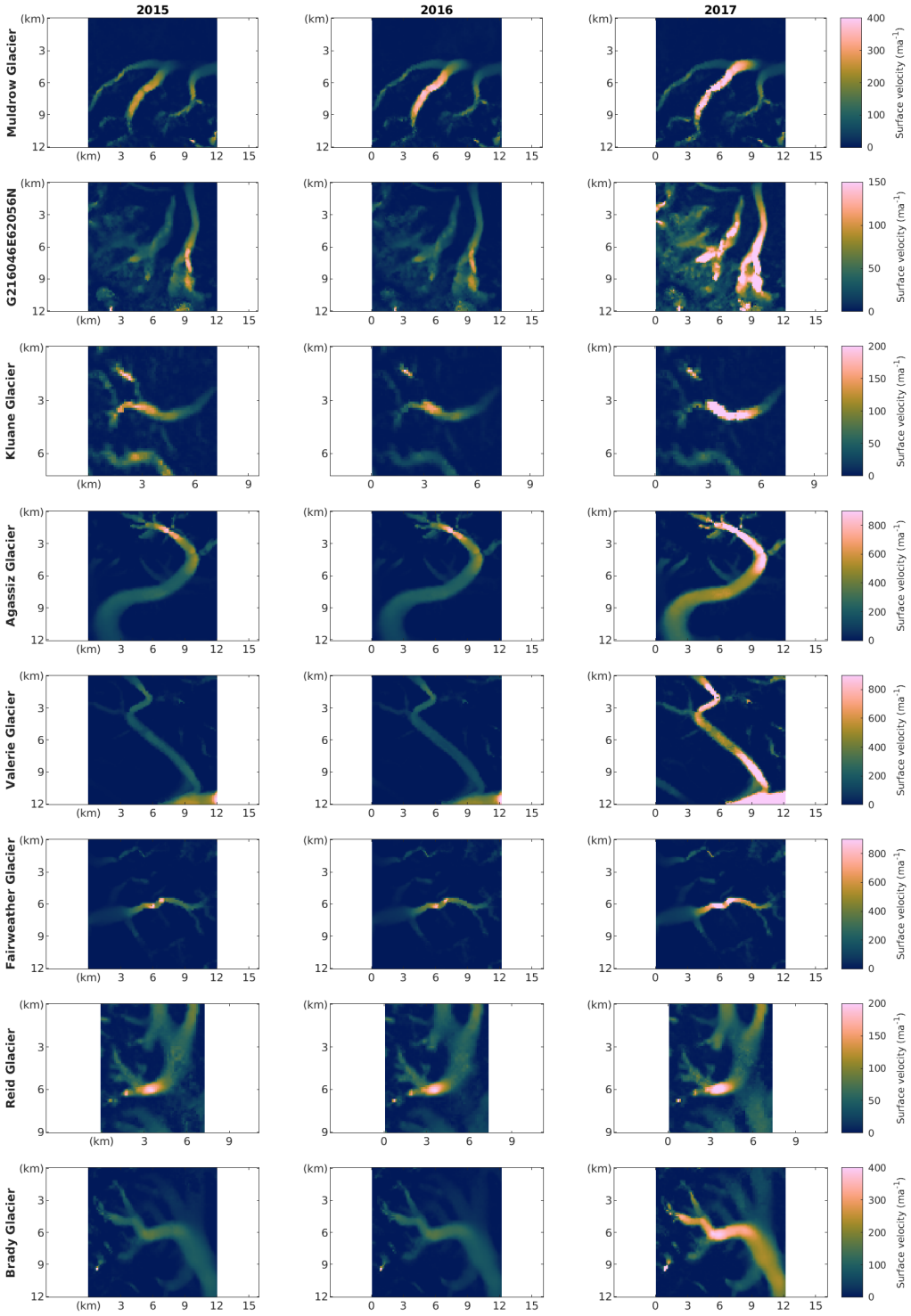

Figure S6: Annual surface velocity for the years 2015 – 2017 in ma^{-1} as provided by ITS_LIVE for the 8 Alaskan glaciers where the radar backscatter increase over the period 2018–2019 suggests surge activity. The images are centered on the glacier of interest. Note that the colour scales can differ for the different glaciers. Colormap is derived from Crameri [2018].

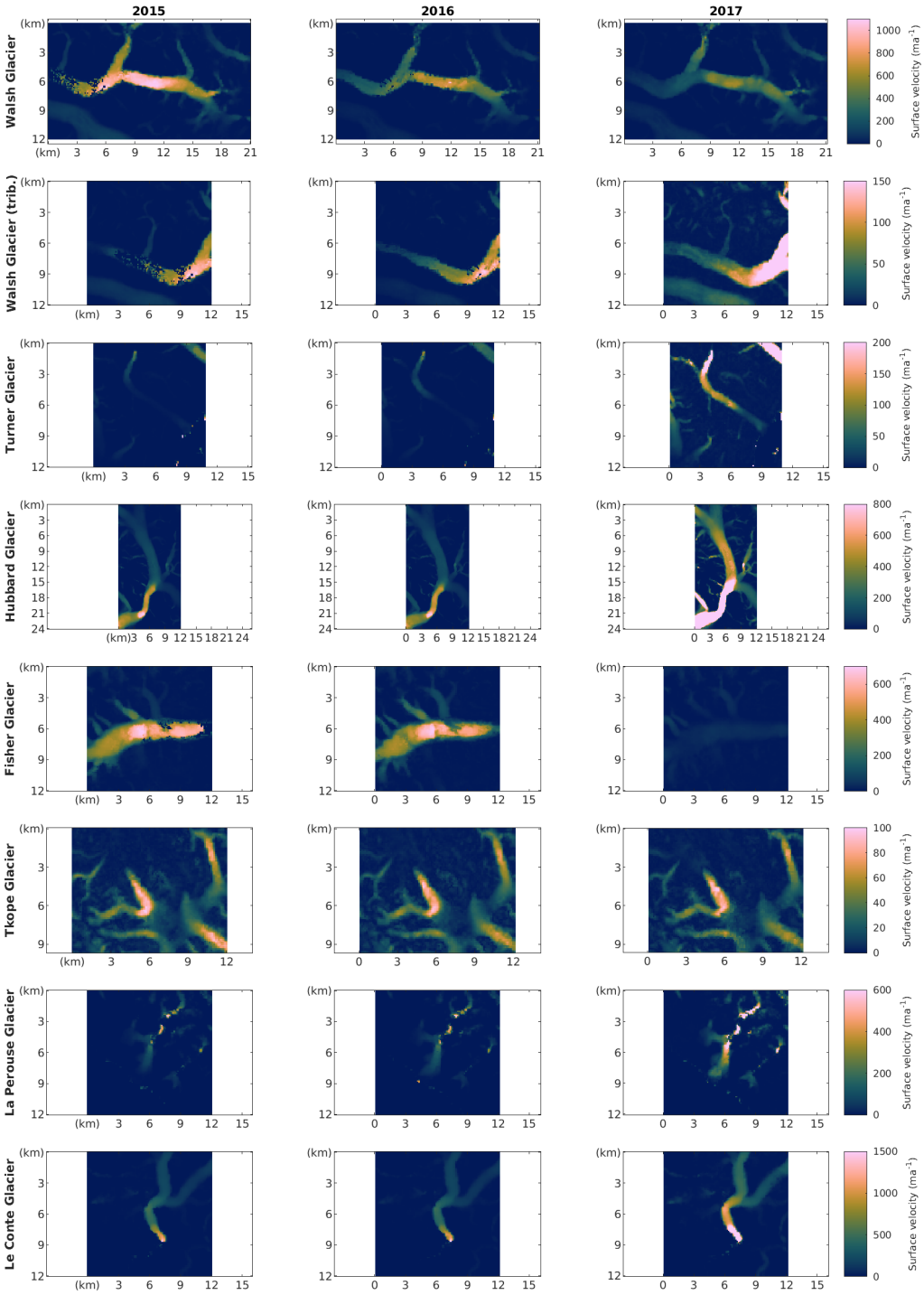

Figure S7: Annual surface velocity for the years 2015 – 2017 in ma^{-1} as provided by ITS_LIVE for the 8 Alaskan glaciers where the radar backscatter decrease over the period 2018–2019 suggests surge activity. The images are centered on the glacier of interest. Note that the colour scales can differ for the different glaciers.

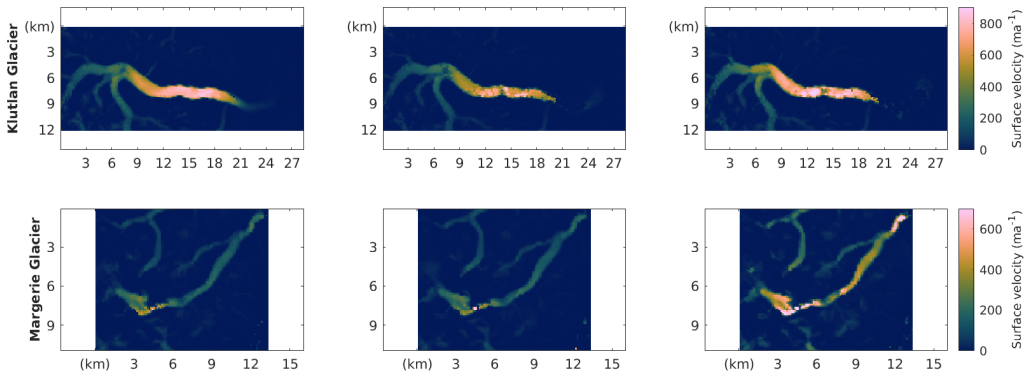

Figure S8: Annual surface velocity for the years 2015 – 2017 in ma^{-1} as provided by ITS_LIVE for the 2 Alaskan glaciers we have observed both increased and decreased radar backscatter in the period 2018-2019 that suggest surge activity.

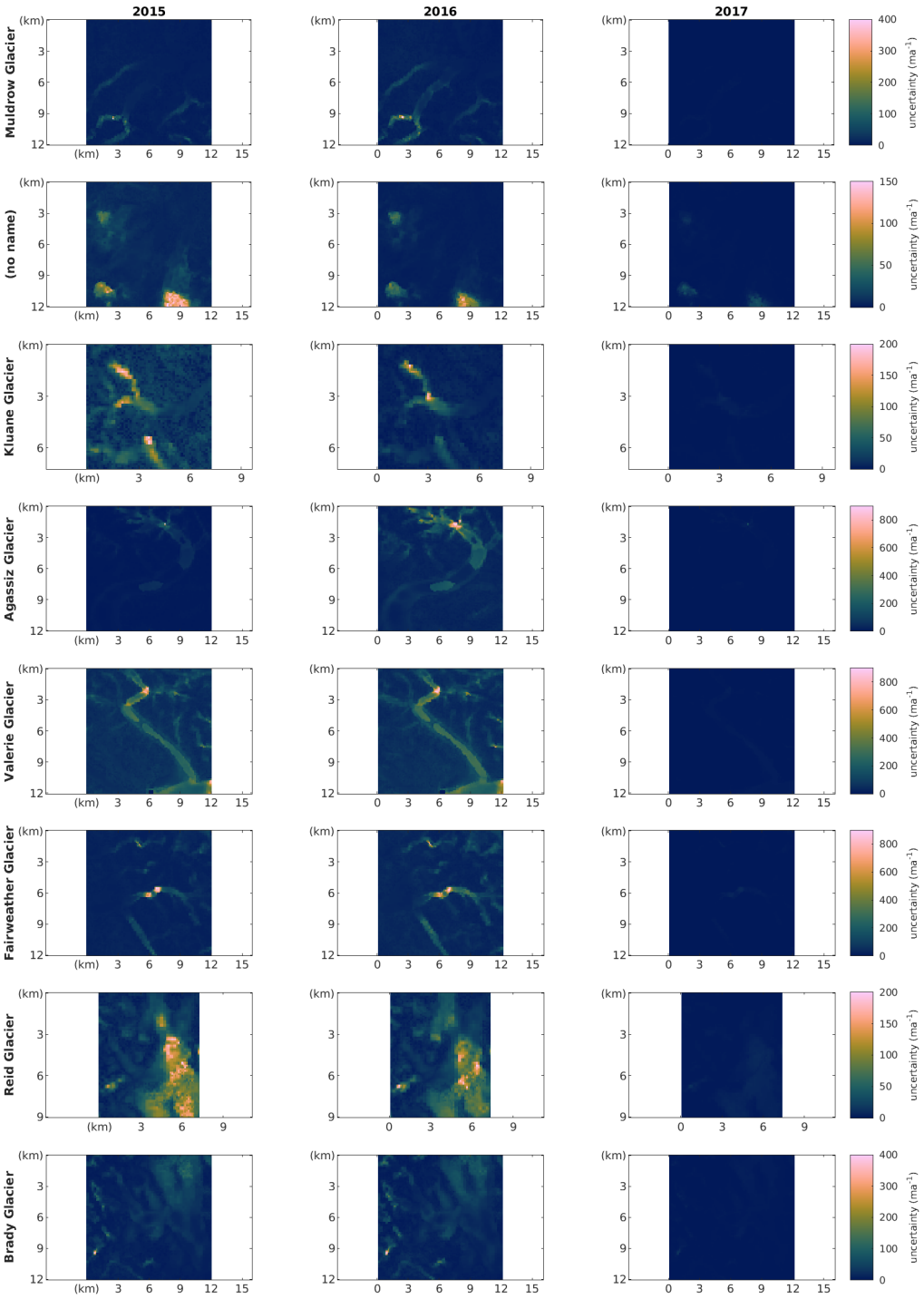

Figure S9: Formal uncertainty in the annual surface velocity for the years 2015 – 2017 in ma^{-1} as provided by ITS_LIVE for the 8 Alaskan glaciers where the radar backscatter increased over the period 2018–2019. Note that the colour scales can differ for the different glaciers.

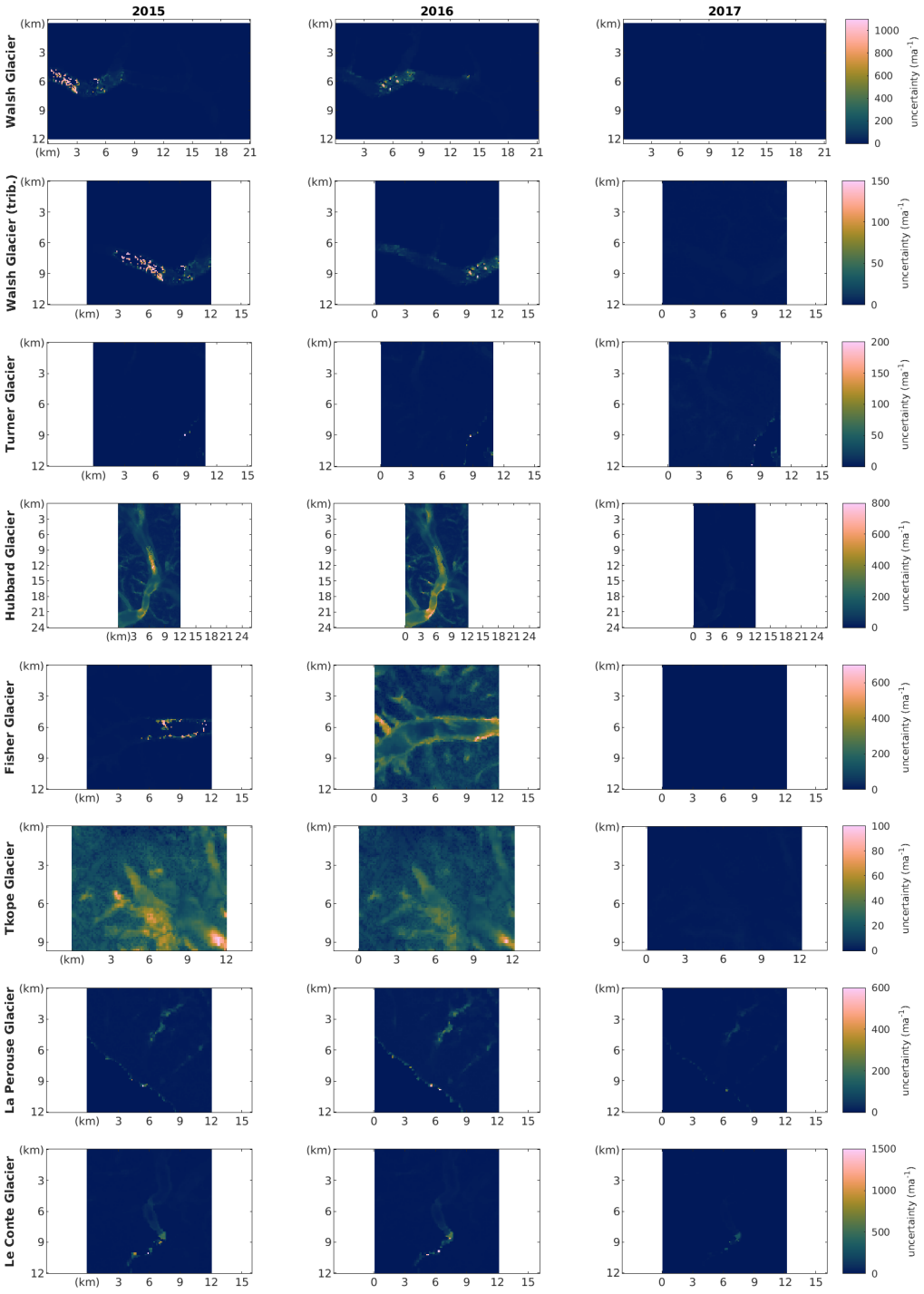

Figure S10: Formal uncertainty in the annual surface velocity for the years 2015 – 2017 in ma^{-1} as provided by ITS_LIVE for the 8 Alaskan glaciers we have observed a decrease in radar backscatter in the period 2018-2019 that suggests surge activity.

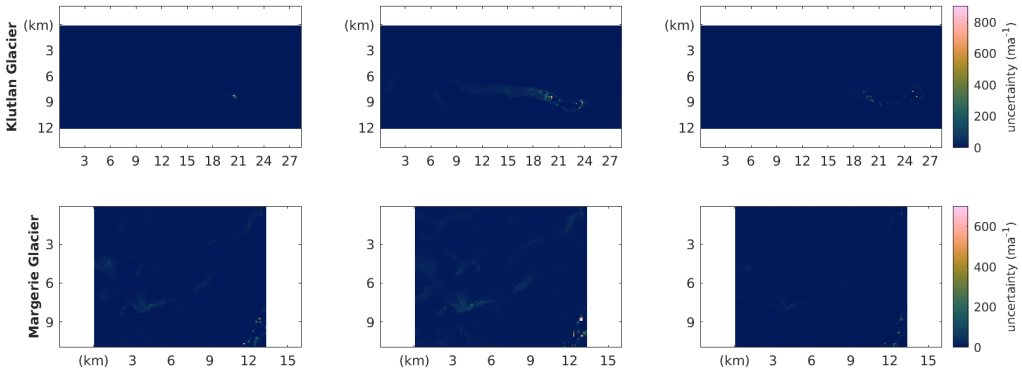

Figure S11: Formal uncertainty in the annual surface velocity for the years 2015 – 2017 in ma^{-1} as provided by ITS_LIVE for the 2 Alaskan glaciers we have observed both increased and decreased radar backscatter in the period 2018-2019 that suggest surge activity.

References

Altena, B., Scambos, T., Fahnestock, M., and Kääb, A.: Extracting recent short-term glacier velocity evolution over southern Alaska and the Yukon from a large collection of Landsat data, The Cryosphere, 13, 795–814, https://doi.org/10.5194/tc-13-795-2019, 2019.

Crameri, F.: Geodynamic diagnostics, scientific visualisation and StagLab 3.0, Geoscientific Model Development, 11, 2541–2562, https://doi.org/10.5194/gmd-11-2541-2018, 2018.

Gardner, A. S., Moholdt, G., Scambos, T., Fahnstock, M., Ligtenberg, S., van den Broeke, M., and Nilsson, J.: Increased West Antarctic and unchanged East Antarctic ice discharge over the last 7 years, The Cryosphere, 12, 521–547, https://doi.org/10.5194/tc-12-521-2018, URL `https://tc.copernicus.org/articles/12/521/2018/`, 2018.

Gardner, A. S., Fahnestock, M. A., and Scambos, T. A.: ITS LIVE Regional Glacier and Ice Sheet Surface Velocities, Data archived at National Snow and Ice Data Center, https://doi.org/10.5067/6II6VW8LLWJ7, 2020.

GLIMS and NSIDC: Global Land Ice Measurements from Space glacier database, Compiled and made available by the international GLIMS community and the National Snow and Ice Data Center, Boulder CO, U.S.A., https://doi.org/10.7265/N5V98602, 2015 (updated 2018).

Kääb, A., Jacquemart, M., Gilbert, A., Leinss, S., Girod, L., Huggel, C., Falaschi, D., Ugalde, F., Petrakov, D., Chernomorets, S., Dokukin, M., Paul, F., Gascoin, S., Berthier, E., and Kargel, J.: Sudden large-volume detachments of low-angle mountain glaciers – more frequent than thought?, The Cryosphere, 15, 1751–1785, https://doi.org/10.5194/tc-15-1751-2021, 2021.

Rashid, I., Majeed, U., Jan, A., and Glasser, N. F.: The January 2018 to September 2019 surge of Shisper Glacier, Pakistan, detected from remote sensing observations, Geomorphology, 351, 106 957, https://doi.org/10.1016/j.geomorph.2019.106957, 2020.

RGI Consortium: Randolph Glacier Inventory - A dataset of Global Glacier Outlines: Version 6.0, Technical Report, Global Land Ice Measurements from Space, Colorado, USA. Digital Media, https://doi.org/10.7265/N5-RGI-60, 2017.

Sevestre, H. and Benn, D. I.: Climatic and geometric controls on the global distribution of surge-type glaciers: implications for a unifying model of surging, Journal of Glaciology, 61, 646–662, https://doi.org/10.3189/2015JoG14J136, 2015.

Strozzi, T., Paul, F., Wiesmann, A., Schellenberger, T., and Kääb, A.: Circum-Arctic Changes in the Flow of Glaciers and Ice Caps from Satellite SAR Data between the 1990s and 2017, Remote Sensing, 9, 947, https://doi.org/10.3390/rs9090947, 2017.